

## Purdue University Purdue e-Pubs

---

International Refrigeration and Air Conditioning  
Conference

School of Mechanical Engineering

---

2018

# Experimental Study on Portable Air-Conditioning System with Enhanced PCM Condenser

Yiyuan Qiao

*Center for Environmental Energy Engineering, University of Maryland, College Park, 4164 Glenn Martin Hall, MD 20742, USA, yyqiao@umd.edu*

Anne Mallow

*Sandia National Laboratories, anne.mallow@gmail.com*

Jan Muehlbauer

*University Of Maryland, United States of America, muehlie@umd.edu*

Yunho Hwang

*yhhwang@umd.edu*

Jiazhen Ling

*University of Maryland, College Park, United States of America, jiazhen@umd.edu*

*See next page for additional authors*

Follow this and additional works at: <https://docs.lib.purdue.edu/iracc>

---

Qiao, Yiyuan; Mallow, Anne; Muehlbauer, Jan; Hwang, Yunho; Ling, Jiazhen; Aute, Vikrant Chandramohan; Radermacher, Reinhard; and Gluesenkamp, Kyle, "Experimental Study on Portable Air-Conditioning System with Enhanced PCM Condenser" (2018). *International Refrigeration and Air Conditioning Conference*. Paper 1986. <https://docs.lib.purdue.edu/iracc/1986>

This document has been made available through Purdue e-Pubs, a service of the Purdue University Libraries. Please contact [epubs@purdue.edu](mailto:epubs@purdue.edu) for additional information.

Complete proceedings may be acquired in print and on CD-ROM directly from the Ray W. Herrick Laboratories at <https://engineering.purdue.edu/Herrick/Events/orderlit.html>

---

**Authors**

Yiyuan Qiao, Anne Mallow, Jan Muehlbauer, Yunho Hwang, Jiazhen Ling, Vikrant Chandramohan Aute, Reinhard Radermacher, and Kyle Gluesenkamp

## Experimental Study on Portable Air-Conditioning System with Enhanced PCM Condenser

Yiyuan QIAO<sup>1</sup>, Anne MALLOW<sup>2</sup>, Jan MUEHLBAUER<sup>1</sup>, Yunho HWANG\*<sup>1</sup>,  
Jiazhen LING, Vikrant AUTE<sup>1</sup>, Reinhard RADERMACHER<sup>1</sup>, Kyle R. GLUESENKAMP<sup>3</sup>

<sup>1</sup>Center for Environmental Energy Engineering,  
Department of Mechanical Engineering, University of Maryland,  
4164 Glenn Martin Hall Bldg., College Park, MD 20742, United States

<sup>2</sup>Thermal/Fluid Sciences and Engineering,  
Sandia National Laboratories, Livermore, CA 94550, United States

<sup>3</sup>Building Equipment Research Group,  
Oak Ridge National Laboratory, Oak Ridge, TN 37831, United States

\*Corresponding author: Tel: (301) 405-5247, email: [yhhwang@umd.edu](mailto:yhhwang@umd.edu)

### ABSTRACT

A portable personal air-conditioning system with a vapor compression cycle (VCC), electrical battery, and thermal battery is an attractive option for localized cooling as compared with stationary air-conditioning systems. A phase change material (PCM) can be used for storing waste heat from the VCC condenser, thereby acting as a thermal battery. In the PCM condenser, copper tubes are submerged in the PCM container. Due to the low thermal conductivity of pure PCM, the overall heat transfer coefficient of the PCM condenser is limited resulting in high VCC condensing pressure and thus, low VCC coefficient of performance (COP). Therefore, it is necessary to improve VCC system performances by applying heat transfer augmentation in PCM. In this work, a portable air-conditioning system with heat transfer enhanced PCM that stores heat from condenser during VCC operation and is regenerated by a thermosyphon operation is proposed. The system also includes a receiver to address the charge difference between the thermosyphon and the VCC operation. The paper experimentally studies the effects of the following three types of enhanced PCM condensers on the system performance: (1) copper mesh enhanced PCM with helically coiled copper tube branches and large refrigerant distribution headers (CMPHX), (2) graphite matrix enhanced PCM with straight copper tube branches and small headers (GMPHX1), and (3) graphite matrix enhanced PCM with straight copper tube branches and large headers (GMPHX2). Results show that this system operates properly and effectively during both VCC and PCM regeneration operations. The system can provide four hours of continuous cooling, and the PCM can be fully regenerated after 7.4 hours by thermosyphon operation. The comparisons of three PCM condensers indicate that the system with GMPHX2 performs the best with the average VCC COP of 4.7. The VCC system with CMPHX has an average COP of 4.2, and GMPHX1 has an average COP of 3.1. GMPHX2 has the best heat transfer enhancement with an overall heat transfer coefficient of  $632.1 \text{ W}\cdot\text{m}^{-2}\cdot\text{K}^{-1}$ , which is more than twice of GMPHX1 and five times of CMPHX. Moreover, GMPHX2 can achieve more uniform refrigerant flows and PCM temperature distributions than GMPHX1. This leads to the higher utilization ratio of PCM latent heat. CMPHX is the second best but needs larger heat transfer surface area and inner volume as well as more refrigerant charge. In conclusion, the system design with GMPHX2 is recommended due to its small refrigerant charge, high VCC COP, and the use of good heat transfer enhancement material.

### 1. INTRODUCTION

The portable personal air-conditioning system is a battery powered thermal comforter equipped with a phase change material (PCM) heat exchanger. This system focuses on providing localized cooling to its user and therefore maintains the user's personal comfort, regardless of building air conditioning thermostat setpoint which may be setback to 4 K+ higher than the conventional setting. By this way, the personal air-conditioning system has the potential to reduce

building energy consumption. The cooling of the system is provided a vapor compression cycle (VCC), in which the PCM absorbs heat from condensing refrigerant and melts into liquid state. Once the PCM is fully melted, the system can turn to thermosyphon operation, in which PCM is solidified by releasing heat to the ambient. Du et al. (2016) experimentally studied the portable air-conditioning system with pure paraffin imbedded condenser, and Dhumane et al. (2018, 2017) simulated it in Dymola and compared with other personal cooling systems. However, the low thermal conductivity of the pure paraffin, which is only  $0.25 \text{ W}\cdot\text{m}^{-2}\cdot\text{K}^{-1}$ , can result in high condensing pressure and low coefficient of performance (COP). Therefore, PCM heat transfer enhancement is required if coupled with the VCC system. Meanwhile, much research has been done to enhance PCM heat transfer in heat exchanger level by associating with various configurations of conductive structures, such as fins (Merlin et al., 2016), metal foam (Yao et al., 2015), graphite powder and compressed expanded natural graphite (Mallow et al., 2018; Medrano et al., 2009). However, the investigation of these types of heat transfer enhanced PCMs applied in VCC systems has not been provided. In this study, the portable personal cooling systems coupled with three different enhanced PCM condensers, including one copper mesh enhanced and two graphite matrix enhanced PCM heat exchangers, are proposed and compared. In the cooling operation, VCC system performances such as condensing pressure, COP, compressor power and PCM temperature distributions, are experimentally studied. Moreover, the PCM regeneration behaviors are discussed in terms of recharge rates and the amount of released thermal energy.

## 2. EXPERIMENTAL SETUP

The experimental setup and schematic diagram are given by Figure 1. To enable the VCC, the three ball valves are closed. In the PCM condenser, heat transfer occurs from refrigerant to PCM through the condenser branch tubes. The selected PCM was PT37 from PureTemp and the melting temperature range is from  $36.5^\circ\text{C}$  to  $37.5^\circ\text{C}$  as specified in Table 1. As the PCM becomes two-phase, the VCC system can take advantage of the heat stored within a limited range of temperature. Once the PCM is completely melted, condensing pressure and condensing temperature start to increase. This leads to a degradation in VCC system performance and thus, a PCM regeneration process is necessary. To properly start a thermosyphon operation, the condenser has to be filled with liquid which requires extra charge than in the VCC operating mode. Therefore, a receiver was installed after the condenser to store the extra amount of refrigerant. The thermosyphon cycle is enabled when three ball valves are open, and the compressor is turned off, so that the liquid refrigerant in the receiver can flow downwards and fill up the PCM condenser. In this case, refrigerant circulates between the condenser and the evaporator while bypassing the compressor and the expansion valve. As ambient temperature is lower than liquid PCM temperature, the PCM condenser works as the heat source, while the upper air-forced heat exchanger works as the heat sink. Owing to the density difference and pressure difference, refrigerant is vaporized after absorbing heat from the PCM and moves upward. Then driven by gravity force, liquid refrigerant condensed from upper heat exchanger, which serves as a thermosyphon condenser, flows to the bottom PCM heat exchanger working as a thermosyphon evaporator, and completes the thermosyphon cycle. No additional pumping power is required.

Three types of PCM condensers were assembled and tested in the system. Each of them consists of a top distribution header, bottom header and copper tube branches with inner diameter (ID) of 4.8 mm in a cylindrical container filled with conductive enhancement mean and PCM. In the VCC cycle, refrigerant flows from the top header to the eight branches and is collected in the bottom header. The selected condensers are as follows:

- Copper mesh enhanced PCM with eight helically coiled copper tube branches and two 7.9 mm ID headers (CMPHX)
- Graphite matrix enhanced PCM with eight straight copper tube branches and two 4.8 mm ID headers (GMPHX1)
- Graphite matrix enhanced PCM with eight straight copper tube branches and two 7.9 mm ID headers (GMPHX2)

The detailed specifications of these PCM condensers are provided in Table 2. The type-T thermocouples with the accuracy of  $0.5^\circ\text{C}$  were placed into PCM at three different heights: the top, middle and bottom layers with top layer located 25 mm below from top, the bottom layer located 25 mm above from bottom. Figure 2 shows the locations of thermocouples in GMPHX1 and GMPHX2. The arrows represent the refrigerant flow directions through the top header (condenser inlet) and the bottom header (condenser outlet). Additional thermocouples were installed at the first several branches near the inlet and last branches near the outlet of PCM condensers.

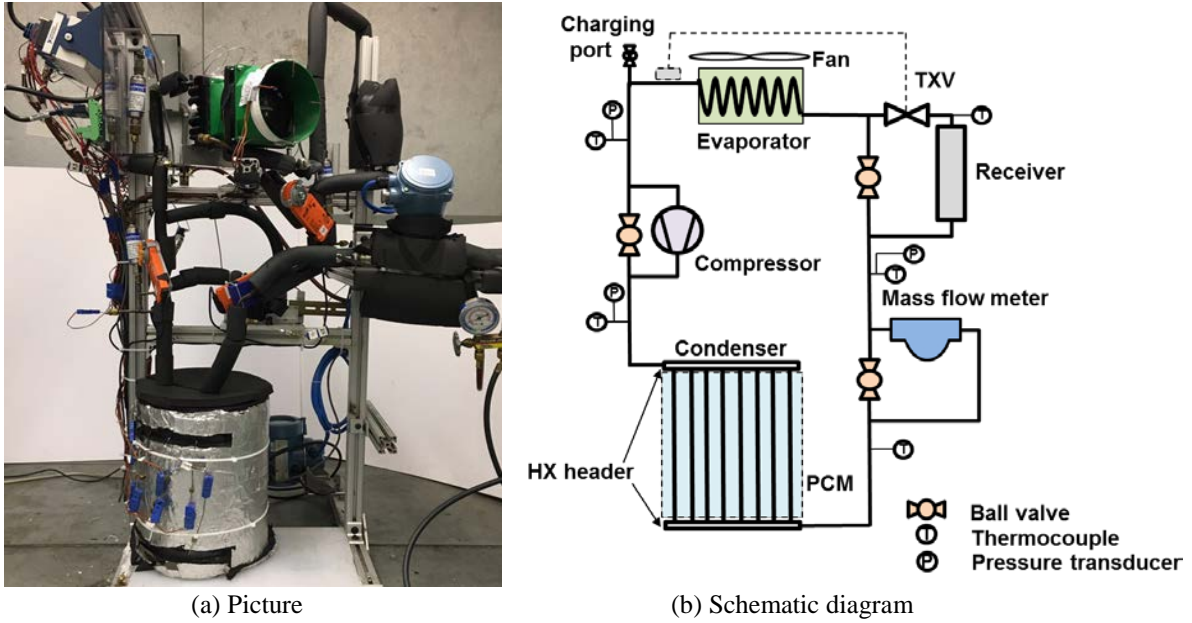


Figure 1: Breadboard system set up

Table 1: Properties of PT37

Properties	Unit	Value
Melting temperature	°C	36.5~37.5
Latent heat	$\text{kJ}\cdot\text{kg}^{-1}$	210
Thermal conductivity	$\text{W}\cdot\text{m}^{-1}\cdot\text{K}^{-1}$	0.15 (liquid), 0.25 (solid)
Density	$\text{kg}\cdot\text{m}^{-3}$	840 (liquid), 920 (solid)
Specific heat	$\text{kJ}\cdot\text{kg}^{-1}\cdot\text{K}^{-1}$	2.63 (liquid), 2.21 (solid)

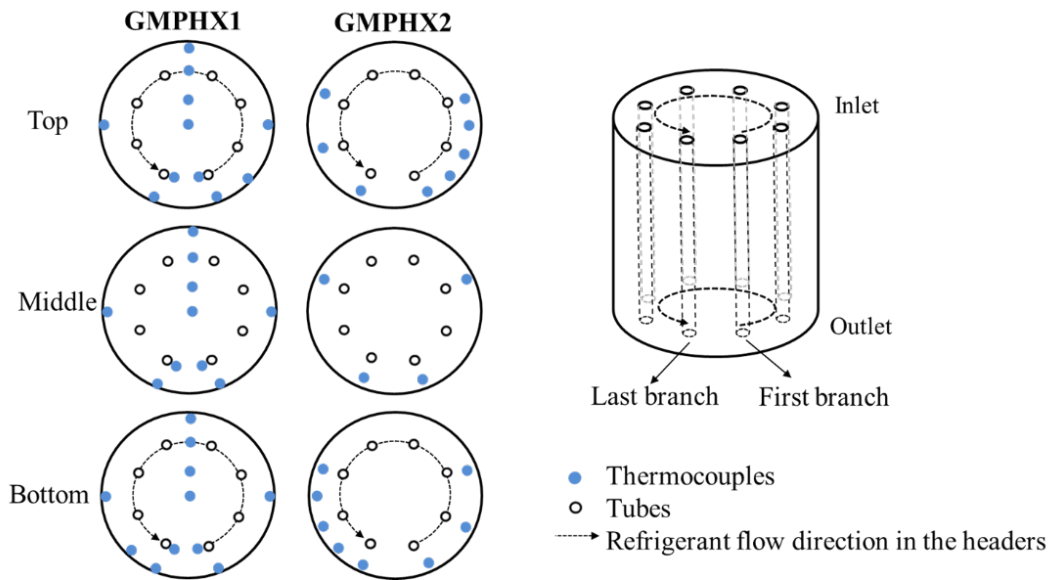



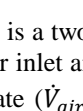


Figure 2: Locations of thermocouples in the PCM condensers

**Table 2:** Dimensions and characteristics of three selected PCM condensers

Designs		M <sub>PCM</sub> (kg)	α <sub>mass</sub> (%)	α <sub>volume</sub> (%)	D <sub>container</sub> (mm)	L <sub>container</sub> (mm)	D <sub>header</sub> (mm)	Branches shape	L <sub>b</sub> (mm)	D <sub>b</sub> (mm)	V <sub>inner</sub> (mL)
CMPHX		16.0	5.5	0.6	300	304	7.9 ID 9.5 OD	Helical	1219	4.8 ID 6.4 OD	211.1
GMPHX1		12.7	12.9	5.2	270	304	4.8 ID 6.4 OD	Straight	304	4.8 ID 6.4 OD	74.8
GMPHX2		11.7	12.9	5.2	270	304	7.9 ID 9.5 OD	Straight	304	4.8 ID 6.4 OD	109.1

The evaporator is a two-row fin-and-tube heat exchanger located at the top of the system. Eight thermocouples were placed at the air inlet and outlet uniformly to obtain the average air temperatures ( $T_{air,in,avg}$  and  $T_{air,out,avg}$ ). The air volume flow rate ( $\dot{V}_{air}$ ) was  $0.038 \text{ m}^3 \cdot \text{s}^{-1}$ . Aspen Q-series rotary compressor with the displacement of 1.4 cc was selected, and the compressor speed was set to be 2,200 RPM. The commercial thermal expansion valve (TXV) was designed to maintain the superheat of 5 K. A Coriolis mass-flow meter from Micro Motion was placed after the condenser with an accuracy of 0.1% of measurement after calibration. According to the inner volume difference of the three PCM condensers, the receiver volume for the system with both GMPHX1 and GMPHX2 was set to 210 mL, while for CMPHX the volume was 350 mL. The data acquisition system using Labview® recorded temperatures and the mass flow rate (MFR) in every 3 s. R134a was chosen as refrigerant in the system.

In the VCC, the instantaneous COP is given by Equation (1) where  $\dot{Q}_e$  and  $W_{comp}$  are evaporator capacity and compressor power, respectively, determined with MFR and enthalpy difference between the inlet and outlet. The average COP of VCC is calculated by Equation (2), where  $\Delta t$  is the recording time interval and  $\dot{Q}_e$  and  $W_{comp}$  are assumed to be constant in  $\Delta t$ . The accumulated energy stored in the PCM during a certain period is given by Equation (3), where  $\dot{Q}_c(t)$  is the condenser capacity.

$$\text{COP}(t) = \frac{\dot{Q}_e(t)}{W_{comp}(t)} \quad (1)$$

$$\text{COP}_{avg} = \frac{\sum \dot{Q}_e(t) \cdot \Delta t}{\sum W_{comp}(t) \cdot \Delta t} \quad (2)$$

$$E_{stored}(t) = \sum \dot{Q}_c(t) \cdot \Delta t \quad (3)$$

The overall heat transfer coefficient (U) when the PCM is in two-phase state is calculated by Equation (4) (Merlin et al., 2016), where  $T_m$  and  $A_c$  are PCM melting temperature and condenser heat transfer area, respectively.

$$U = \frac{\sum \dot{Q}_c(t) \cdot \Delta t}{\sum (T_{c,sat}(t) - T_m) \cdot A_c} \quad (4)$$

In the thermosyphon operation, evaporator and condenser capacities are assumed to be same by ignoring the heat loss from the connecting pipes, which is also equal to the heat release rate in Equation (5). The accumulated heat released from PCM is calculated by Equation (6). The PCM regeneration fraction is defined to evaluate the ratio of the PCM recharge process in Equation (7), which is determined by the released heat at a certain time and the total heat stored in the PCM in the VCC cycle. In this equation,  $t_{tot}$  is the VCC total operation time.

$$\dot{Q}_{recharge}(t) = \rho_{air} \dot{V}_{air} C_{p,air} (T_{air,in,avg}(t) - T_{air,out,avg}(t)) \quad (5)$$

$$E_{released}(t) = \sum \dot{Q}_{recharge}(t) \cdot \Delta t \quad (6)$$

$$\gamma(t) = \frac{E_{stored}(t)}{E_{released}(t_{tot})} \quad (7)$$

### 3. RESULT AND DISCUSSION

The experimental study of the air-conditioning system coupled with three types of enhanced PCM condensers was performed in the environmental chamber. The ambient temperature was set to be 26°C. The performances of VCC cycle and PCM recharge cycle were evaluated.

#### 3.1 Cooling operation

##### 3.1.1 VCC System performance

Heat transfer occurs between the refrigerant and the PCM in the condenser. Absorbing heat from refrigerant, PCM undergoes dynamic process in which its state and temperature continuously change with the operation time. In the experiment, subcooled solid PCM temperature increased at the beginning of VCC operation, and then PCM temperature during the melting process stayed at a nearly constant temperature, and finally the PCM temperature start to increase after melting into liquid phase completely. This dynamic process would lead to the change of the condensing temperature as well as system performances at different operation periods.

The trends of VCC evaporating pressure and condensing pressure are given in Figure 3. The evaporating pressures of the system with different condensers were same because of the stable air inlet temperature and the proper function of TXV. For the system with CMPHX, condensing pressure increased during first 30 minutes due to the increase of the PCM temperature. During this period, thermal energy was stored in the form of sensible heat of the solid PCM. Then, its condensing pressure remained constant at 1,160 kPa, while condensing pressures of GMPHX1 and GMPHX2 increased slowly. It was obvious that CMPHX had constant condensing temperature when PCM was in two-phase state, but for two GMPHXs, the constant condensing pressures were never found. The reason of this difference might be the different heat transfer mechanisms in copper mesh and graphite matrix enhanced PCM. Free convection has a significant augmentation of heat transfer in liquid PCM within copper foam (Liu et al., 2006; Tay et al., 2013). When the PCM close to the wall of branches began to melt, it could keep nearly constant temperature until the PCM far from the wall melted completely, due to the free convective motion of the liquid PCM (Longeon et al., 2013). So, the condensing temperature of CMPHX could keep constant during this period. However, for the graphite enhanced PCM, free convection could be ignored because of absence of liquid movement due to the higher volume fraction of graphite foam (Chen et al., 2016). Thus, the heat transfer was dominated by conduction, and temperature of PCM close to the tube wall of the branches increased faster than the PCM far from the tubes leading to the increase of the condensing temperature.

It can also be seen from Figure 3 that condensing pressure of CMPHX was higher than GMPHX2 during first 3 hours. One reason for this could be that the effective thermal conductivity of graphite foam is higher than the copper mesh (Medrano et al., 2009), even though the active heat transfer areas of CMPHX is three times larger than GMPHX2. However, after 3.5 hours, the condensing pressure of GMPHX2 increased much faster than before, while the pressure of CMPHX increased slowly till the end of operation time. The mass of PCM within CMPHX is 26% more than GMPHX2, so after 3.5 hours, most PCM melted into liquid state in GMPHX2, while PCM was still in two-phase state in CMPHX resulting in the lower condensing temperature and pressure.

Figure 3 also presents that condensing pressures of two graphite enhanced condensers were different. The condensing pressure of GMPHX1 (red dash line) was more than 200 kPa higher than GMPHX2 (green line), and the increase rate of GMPHX1 was more pronounced during first 3 hours. This is because of the maldistribution of refrigerant flows among eight branches of GMPHX1 resulting in non-uniform PCM temperatures close to branches. In the VCC, refrigerant from top header (inlet) flowed to eight branches successively and was collected at bottom header (outlet). The headers of GMPHX1 had the same inner diameter with branches, so more refrigerant flowed into the first several branches due to the less pressure drop. The PCM near first several branches that had more refrigerant flow melted faster than the last branches with less refrigerant flow, and thus, PCM temperatures around first several branches were

higher than the rest of the branches. These temperatures were verified in Figure 4. For example, at 2.5 hours, PCM temperatures near first three branches at top layer were 43.8°C, 46.0°C and 47.2°C, respectively, while the temperatures near last three branches were only 36.6°C and 35.7°C. This maximum temperature difference was 11.5 K. However, as for GMPHX2, this temperature difference was less than 1 K in advantage of the bigger headers, leading to the uniform distribution of refrigerant flows in eight branches. As most of the condenser capacity of CMPHX2 was accomplished by the first several branches, condensing temperature and pressure had to increase rapidly to match the PCM temperature at these locations. Thus, the condensing pressure of the system with GMPHX1 was higher than that with GMPHX2. As the PCM near each branch within GMPHX2 discharged with similar melting rate, it can also be concluded that GMPHX2 has higher utilization ratio of PCM latent heat.

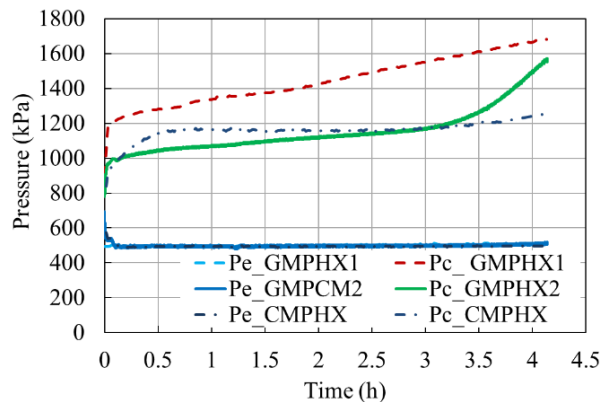


Figure 3: VCC pressures of the systems with GMPHX1, GMPHX2 and CMPHX

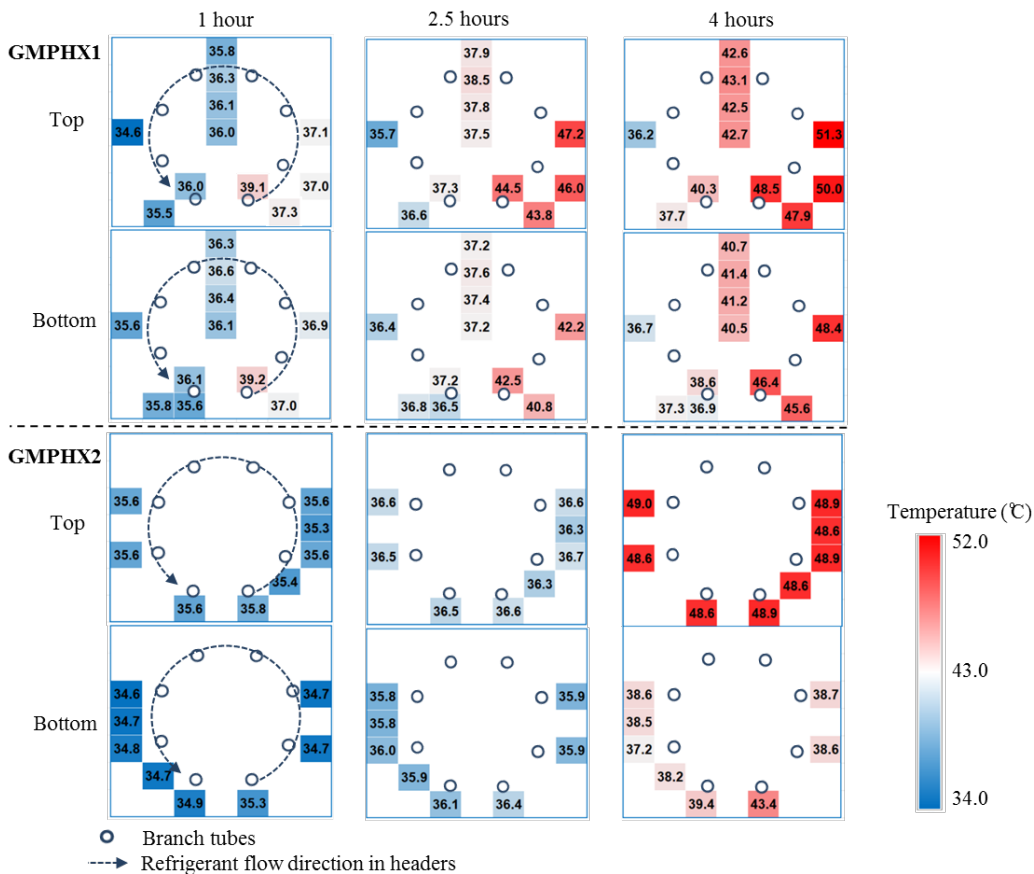


Figure 4: GMPHX1 and GMPHX2 temperature profiles of top and bottom layers at 1, 2.5 and 4 hours in VCC

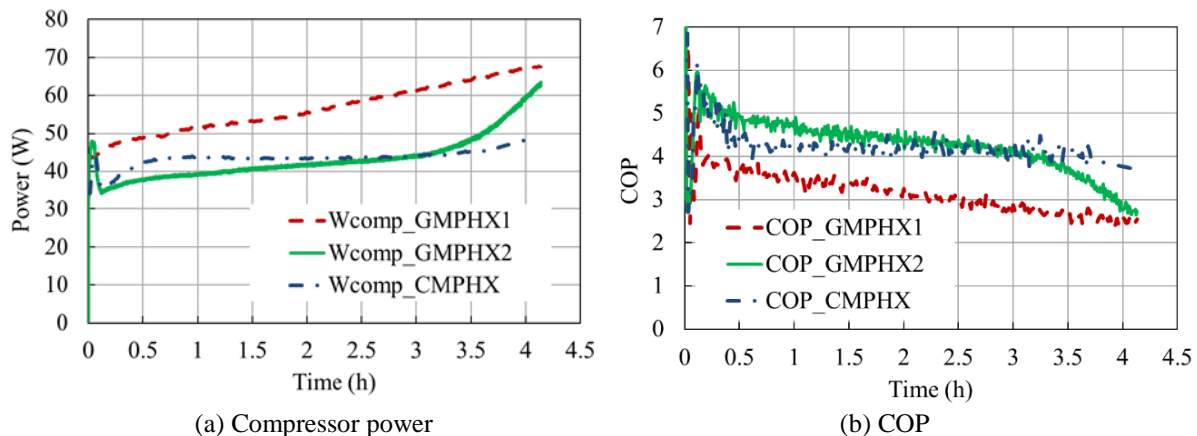


Refrigerant mass flow rates (MFR) and evaporator capacities with three types of condensers are given in Table 3. The refrigerant MFR of the system with CMPHX was constant, while that of GMPHX1 and GMPHX2 decreased with operation time. This is because the increased condensing pressure can lead to the drop of the compressor volumetric efficiency due to higher compression ratio. As for the evaporator capacities, it decreased with the decline of refrigerant MFR. On the other hand, the increase of the discharge pressure also decreased the enthalpy difference between the evaporator inlet and the outlet. Hence, the evaporator capacities of CMPHX remained nearly constant, while that of GMPHX2 changed slightly and that of GMPHX1 decreased gradually. As the change of evaporator capacities of the systems with the three condensers was less than 10% during the cooling operation time, it can be concluded that the cooling mode of this air-conditioning system coupled with enhanced PCM condenser can work properly.

Figure 5 presents the compressor power and instantaneous COP during the cooling operation. Owing to the stable evaporating pressures and superheat, compressor power tendencies were similar to condensing pressure trends. Moreover, the system with CMPHX had a constant COP of 4.2 for 80% of the cooling operation time. For GMPHX2, instantaneous COP decreased gradually from 6.0 to 4.1 during first 3 hours, which mainly resulted from the increased compressor power consumption. And as for GMPHX1, instantaneous COP was lower than the other two condensers due to the increased compressor work and the decreased evaporator capacity. To evaluate the system performance during the cooling operation, accumulated evaporator energy ( $\sum \dot{Q}_e(t) \cdot \Delta t$ ) and compressor energy consumption ( $\sum W_{comp}(t) \cdot \Delta t$ ) were applied to calculate average COP. Because the mass of the PCM in these three condensers was different, average COP is calculated over the first 3 hours prior to the PCM becoming fully liquid state. The average COP of VCC during the first 3 hours with CMPHX, GMPHX1 and GMPHX2 were 4.2, 3.1 and 4.7, respectively. These results suggest that GMPHX2 performed the best in terms of system level.

**Table 3:** Refrigerant mass flow rates and evaporator capacities of systems with three PCM condensers

PCM HX design	MFR				Evaporator capacity			
	1 hour	2 hours	3 hours	4 hours	1 hour	2 hours	3 hours	4 hours
CMPHX	1.08	1.07	1.07	1.07	185	185	184	184
GMPHX1	1.05	1.02	1.00	0.98	179	175	170	164
GMPHX2	1.08	1.08	1.08	1.03	185	185	184	173



**Figure 5:** Compressor power and COP of three types of condensers during cooling operation period

### 3.1.2 PCM condenser comparisons

As the system performances changed with operation time and PCM states, the heat exchanger-level comparisons are based on the condition in which PCM is in two-phase state. Figure 6 illustrates the summary of the three PCM condensers performances. The inner volume of GMPHX2 is only the half of the CMPHX. Also, GMPHX2 has the lowest condensing temperature of 42.8°C and the highest UA of 30.9 W·K<sup>-1</sup>. Its overall heat transfer coefficient is 632.1 W·m<sup>-2</sup>·K<sup>-1</sup>, which is more than twice of GMPHX1 and five times of CMPHX. Thus, it can be concluded that GMPHX2 demonstrated the best heat exchanger performance of the three designs. CMPHX is the second best with a UA of 23.7 W·°C<sup>-1</sup> but has large inner volume requiring larger amount of refrigerant charge.

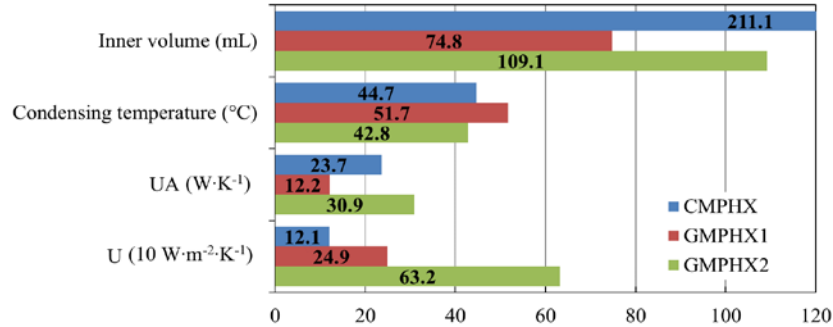


Figure 6: Comparisons of PCHX, GMPHX1 and GMPHX2 when PCM is in two-phase state

### 3.2 PCM regeneration operation

Thermosyphon cycle operates for PCM regeneration. Figure 7 demonstrates the air inlet and outlet temperatures of the air-to-refrigerant heat exchanger in the system with GMPHX1 during thermosyphon cycle. The outlet air temperature decreased rapidly during first 30 minutes, because most liquid PCM released sensible heat leading to the decrease of the approaching temperature difference between refrigerant and PCM. At 0.5 hours, PCM began to be in two-phase state. From 0.5 hours to 6 hours, this air outlet temperature dropped with slow rate due to limited temperature range of the two-phase PCM. During the rest of recharge time, PCM was in the solid state, so the air outlet temperature decreased gradually. At 7.4 hours, the air temperature difference between inlet and outlet remained constant at 0.3 K rather than being 0 K. The reasons for this could be the thermocouples measurement uncertainty, which is 0.5 K, and the heat from the fan motor. Therefore, it can be concluded that at 7.4 hours, PCM regeneration cycle with GMPHX1 was finished. The PCM regeneration fraction and released heat from the PCM with two-hour intervals are presented in Table 4. The recharged fraction was not 100% due to the heat loss to ambient from VCC and thermosyphon loop. In addition, the higher air outlet temperature resulted from the higher heat exchanger capacity which is equal to heat release rate (see Figure 8). The heat release rate of CMPHX was lower than GMPHX1 and GMPHX2 due to its lower effective conductivities with the deficiency of free convection in the solidification process (Longeon et al., 2013). The heat release rates of GMPHX1 and GMPHX2 were similar when PCM was in two-phase, which implies that the size of the PCM heat exchanger headers played a minor role on thermosyphon performance. Also, the heat release rate could be limited by refrigerant side in PCM heat exchanger and upper heat exchanger.

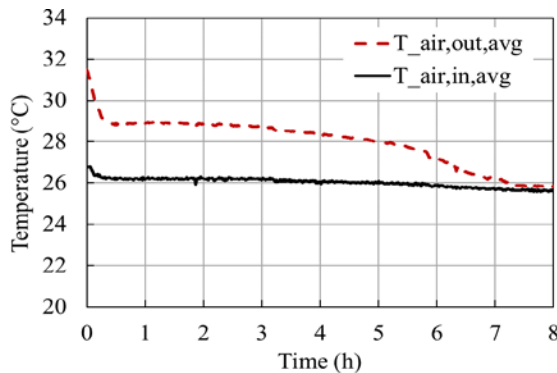


Figure 7: Air inlet and outlet temperatures of upper heat exchanger in thermosyphon loop with GMPHX1

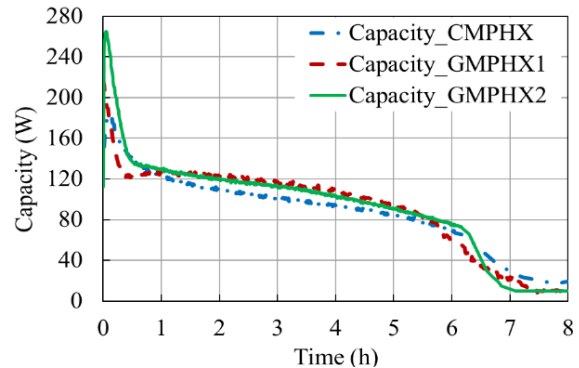


Figure 8: Capacities of three types of PCM heat exchangers in thermosyphon operation

Table 4: PCM regeneration fraction and released thermal energy in thermosyphon loop at five operation periods

Regeneration time (h)	CMPHX		GMPHX1		GMPHX2	
	$E_{released}$ (kJ)	$\gamma$ (%)	$E_{released}$ (kJ)	$\gamma$ (%)	$E_{released}$ (kJ)	$\gamma$ (%)
0	0	0	0	0	0	0
2	915	31	942	33	1026	34
4	1653	56	1771	62	1872	62
6	2272	77	2428	85	2536	84
8	2479	84	2599	91	2687	89

## 4. CONCLUSIONS

In this paper, the portable air-conditioning system with PCM condenser is designed and experimentally studied. Both the cooling operation by VCC and the PCM regeneration cycle by thermosyphon are investigated. Experimental results show that this air-conditioning system coupled with PCM can work properly in both operations. Cooling operation time is more than 4 hours, while PCM recharge time is 7.4 hours. In the system level study of cooling operation, VCC system characteristics with CMPHX, such as compressor power, condensing pressure and COP, are stable during 80% of operation time, while with GMPHX1 and GMPHX2 gradually decrease. GMPHX2 have the highest average COP of 4.7. And the average COP of CMPHX is 4.2 and of GMPHX1 is 3.1. Also, in VCC, GMPHX2 with large headers could achieve more uniform refrigerant flows and PCM temperature distributions than GMPHX1 with small headers. In the heat exchanger level study, when PCM is in two-phase state, the comparison indicates that GMPHX2 presents the best performance with the highest U value of  $632.0 \text{ W}\cdot\text{m}^{-2}\cdot\text{K}^{-1}$ , the highest UA of  $30.9 \text{ W}\cdot\text{K}^{-1}$  and relatively small inner volume. CMPHX is the second best with UA of  $23.7 \text{ W}\cdot\text{K}^{-1}$  and larger inner volume resulting in the need of larger volume of receiver and more refrigerant charge. As for thermosyphon based PCM regeneration, heat release rate of CMPHX is slightly lower than GMPHX1 and GMPHX2 when PCM is two-phase, and the size of heat exchanger headers plays a minor role. In conclusion, the system design with GMPHX2 is recommended because of its highest average VCC COP, highest UA and reasonable refrigerant charge.

## NOMENCLATURE

A	heat transfer area	( $\text{m}^2$ )
C	specific heat	( $\text{J}\cdot\text{g}^{-1}\cdot\text{K}^{-1}$ )
E	energy	(J)
ID	inner diameter	(mm)
L	length	(mm)
M	mass	(kg)
MFR	mass flow rate	( $\text{g}\cdot\text{s}^{-1}$ )
OD	outer diameter	(mm)
$\dot{Q}$	capacity	(W)
t	time	(s)
T	temperature	( $^{\circ}\text{C}$ )
U	overall heat transfer coefficient	( $\text{W}\cdot\text{m}^{-2}\cdot\text{K}^{-1}$ )
UA	overall thermal conductance	( $\text{W}\cdot\text{K}^{-1}$ )
V	volume flow rate	( $\text{m}^3\cdot\text{s}^{-1}$ )
W	power	(W)

### Greek

$\alpha$	fraction of the enhancement	(-)
$\gamma$	recharge fraction	(%)
$\rho$	density	( $\text{kg}\cdot\text{m}^{-3}$ )

### Subscript

air	air side	m	PCM melting
avg	average value	mass	total mass of PCM and enhancement
c	condenser	out	outlet
comp	compressor	released	released from PCM
container	PCM container	sat	saturation
e	evaporator	stored	stored in PCM
header	headers of PCM heat exchangers	tot	total
HX	PCM heat exchanger	tube	copper branch tubes in PCM condenser
in	inlet	volume	total mass of PCM and enhancement

## REFERENCES

- Chen, C., Zhang, H., Gao, X., Xu, T., Fang, Y., and Zhang, Z. 2016. Numerical and experimental investigation on latent thermal energy storage system with spiral coil tube and paraffin / expanded graphite composite PCM. *Energy Conversion and Management*, vol. 126: pp. 889–897.
- Dhumane, R., Ling, J., Aute, V., and Radermacher, R. 2017. Portable personal conditioning systems: Transient modeling and system analysis. *Applied Energy*, vol. 208, no. July: pp. 390–401.
- Dhumane, R., Mallow, A., Qiao, Y., Gluesenkamp, K. R., Graham, S., Ling, J., and Radermacher, R. 2018. Enhancing the Thermosyphon-Driven Discharge of a Latent Heat Thermal Storage System used in a Personal Cooling Device. *International Journal of Refrigeration*.
- Du, Y., Muehlbauer, J., Ling, J., Aute, V., Hwang, Y., and Radermacher, R. 2016. Rechargeable personal air conditioning device. *ASME 2016 10th International Conference on Energy Sustainability, ES 2016, Collocated with the ASME 2016 Power Conference and the ASME 2016 14th International Conference on Fuel Cell Science, Engineering and Technology*, vol. 1: pp. 1–5.
- Liu, Z., Wang, Z., and Ma, C. 2006. An experimental study on heat transfer characteristics of heat pipe heat exchanger with latent heat storage. Part I: Charging only and discharging only modes. *Energy Conversion and Management*, vol. 47, no. 7–8: pp. 944–966.
- Longeon, M., Soupart, A., Fourmigué, J.-F., Bruch, A., and Marty, P. 2013. Experimental and numerical study of annular PCM storage in the presence of natural convection. *Applied Energy*, vol. 112: pp. 175–184.
- Mallow, A., Abdelaziz, O., and Graham, S. 2018. Thermal charging performance of enhanced phase change material composites for thermal battery design. *International Journal of Thermal Sciences*, vol. 127, no. November 2017: pp. 19–28.
- Medrano, M., Yilmaz, M. O., Nogués, M., Martorell, I., Roca, J., and Cabeza, L. F. 2009. Experimental evaluation of commercial heat exchangers for use as PCM thermal storage systems. *Applied Energy*, vol. 86, no. 10: pp. 2047–2055.
- Merlin, K., Delaunay, D., Soto, J., and Traonvouez, L. 2016. Heat transfer enhancement in latent heat thermal storage systems: Comparative study of different solutions and thermal contact investigation between the exchanger and the PCM. *Applied Energy*, vol. 166: pp. 107–116.
- Tay, N. H. S., Belusko, M., Bruno, F., Martinelli, M., Bentivoglio, F., Caron-Soupart, A., ... Abdelrahman, W. 2013. Experimental and numerical study of annular PCM storage in the presence of natural convection. *Applied Energy*, vol. 112, no. November 2016: pp. 175–184.
- Yao, Y., Wu, H., and Liu, Z. 2015. A new prediction model for the effective thermal conductivity of high porosity open-cell metal foams. *International Journal of Thermal Sciences*, vol. 97: pp. 56–67.

## ACKNOWLEDGEMENT

This research was supported by the Advanced Research Projects Agency - Energy (ARPA-E) under Award DE-AR0000530 and Center for Environmental Energy Engineering (CEEE). The authors acknowledge the support of the team members of the Roving Comforter Project.

Notice: This manuscript has been co-authored by UT-Battelle, LLC, under contract DE-AC05-00OR22725 with the US Department of Energy (DOE). The US government retains and the publisher, by accepting the article for publication, acknowledges that the US government retains a nonexclusive, paid-up, irrevocable, worldwide license to publish or reproduce the published form of this manuscript, or allow others to do so, for US government purposes. DOE will provide public access to these results of federally sponsored research in accordance with the DOE Public Access Plan (<http://energy.gov/downloads/doe-public-access-plan>).